Graphene based Low Voltage Field Effect Transistor Coupled with Biodegradable Piezoelectric Material based Dynamic Pressure Sensor

*Nivasan Yogeswaran, Ensieh S. Hosseini, Ravinder Dahiya**

Bendable Electronics and Sensing Technologies (BEST) Group, James Watt School of Engineering, University of Glasgow, G12 8QQ, Glasgow, UK.

ABSTRACT: Pressure sensors form the basic building block for realisation of an electronic or tactile skin used in prothesis, robotics and other similar applications. This paper presents a device consisting of biodegradable piezoelectric material based dynamic pressure sensor coupled with a graphene field-effect-transistor (GFET) operated at very low voltage (50mV). The device has a biodegradable β-glycine/chitosan composite based metal-insulator-metal (MIM) structure connected with GFET in an extended gate configuration. The developed device shows a sensitivity of 2.70×10^{-4} kPa^{-1} for a pressure range of 5 - 20 kPa and 7.56×10^{-4} kPa^{-1} for a pressure range between 20-35 kPa. A distinctive feature of the presented device is its very low operation voltage, which offers a significant advantage towards the development of energy efficient large-area electronic skin. Further, the biodegradability of piezoelectric material makes presented sensors useful in terms of reduced electronic waste, which is current another growing area of interest.

KEYWORDS: GFET, biodegradable pressure sensor, Glycine, piezoelectric transducer layer, electronic skin, Low voltage transistor .

Introduction

Pressure sensors are key to the electronic skin (eSkin) and its application in prosthesis, robotics and wearables [1-2]. Amongst different strategies investigated for the fabrication of the pressure sensors, the field effect transistor (FET) based approach has garnered significant interest due to advantages such as low signal-noise ratio, high sensitivity, high spatial resolution of sensors and possibility to realise active matrix [3-5]. The FETs based on standard silicon technology as well as organic semiconductors have been explored in literature with pressure sensing layer as part of device structure or connected in an extended gate configuration [6-7]. The organic materials based FETs are intrinsically flexible but often suffer from high operation voltage and low carrier mobility [8-10]. Our earlier work on graphene FET (GFET) addressed some of the key issues associated with organic FETs [11].

In relation with the pressure sensing layer, various piezoelectric material such as the polyvinylidene fluoride (PVDF) and co-polymer (PVDF-TrFE) [6, 12], lead zirconate titanate (PZT) [11, 13], zinc oxide (ZnO) [14-15], lead titanate nanowires [16], and aluminium nitride (AlN) [17] etc. have been explored with FETs for dynamic pressure sensing. Among these, PVDF, (PVDF-TrFE) and PZT have been extensively studied and often they require a high voltage (100kV/cm) poling process for enhanced piezoelectric property. Such high-voltages could unfavourably impact the device performance and may even damage the FETs. In this respect, the use of the structurally piezoelectric material such as aluminium nitride (AlN), where poling step is not needed, have also been explored. The CMOS compatibility of AlN also offers a significant advantage over the aforementioned piezoelectric materials [18]. The bio-based natural piezoelectric materials such as β-glycine are even more attractive, owing to their unique feature such as biodegradability and superior piezoelectric properties [19-21]. The ease of synthesis, room

temperature processing, biocompatibility and low cost are additional advantages of β-glycine, which is also known to exhibit a high piezoelectric coefficient (e.g. d_{16}= 174 pm/V and d_{22}= -5.7 pm/V) [22]. However, due to the instability of β-glycine under ambient conditions, their application has been limited. Nonetheless, this issue could be resolved by fabricating a composite of glycine with biodegradable dielectric polymers, so as to provide the required stability while retaining the piezoelectric properties. This is achieved by crystallization of glycine molecules in the chitosan polymer matrix using simple and inexpensive solution casting method [21].

Taking advantage of these benefits, here we present a dynamic pressure sensor comprising of biodegradable β-glycine/chitosan composite piezoelectric transducer layer coupled with graphene field effect transistor (GFET) (Fig.1). The β-glycine/chitosan composite based metal-insulator-metal (MIM) structure is used here as the extended gate of GFET as this configuration restricts the mechanical inputs to transducer only and prevents any pressure stimuli related variation in GFET electrical response. Further, the extended gate configuration also addresses the current limitation related to the poor adhesion of the β-glycine/chitosan to the substrate. The presented device operates at significantly low voltage (50 mV), opening an avenue towards the development of the low power sensors for applications such as wearables. In addition, such sensors could be scaled up towards the development of the high resolution sensors with low noise which are attractive feature for the development of large area eSkin. The paper is strucutred as follows: section II discusses the fabrication process and the experimental methodology related to the characterisation of the pressor sensor. The results of the β-glycine/chitosan (β-Gly/CS) film and the pressure sensor characterisation are presented in the section III. Finally, the key results are summarised in the conclusion section.

Experimental Section

2.1. Synthesis of glycine composite and fabrication of transducer MIM structure

The biodegradable piezoelectric film was synthesised using glycine powder and low molecular weight chitosan (both from Sigma Aldrich). Glycine/chitosan solutions were prepared by dissolving 0.8: 1 (w/w) glycine to chitosan in an aqueous 1% v/v acetic acid solution. The resulting glycine/chitosan viscuss solution was casted on a 100 nm thick Au coated Si substrate. The crystallisation of the glycine/chitosan film was carried over room temperature for two days. The 0.8:1 (w/w) has been used here, as this is the optimum glycine to chitosan ratio leading to development of uniform films with significant piezoelectricity, as reported in our previous work[21]. The surface morphology and crystalline structure of the synthesised glycine/chitosan composite film were studied by optical microscopy (Nikon, Eclipse LV100ND) and x-ray diffraction (XRD, PANalytical X'Pert Pro-MPD diffractometer) respectively. The microstructure of the glycine/chitosan composite films were studied by scanning electron microscopy (SEM, FEI Nova Nano). The results of the analysis are presented in the subsequent section. The poor adhesion between the Si/Au substrate and glycine/chitosan film aided the removal of the bio-organic film from the Si substrate. Eventually, the β-Gly/CS film was sandwiched between two Cu electrodes and encapsulated by a thin layer of PDMS film. The fabricated glycine/chitosan film and MIM structure are shown in Fig 2.

2.2. Fabrication process for Active device (GFET)

One of the vital step in development of GFET is the transfer of graphene to a suitable substrate. In this study, a wet transfer process employing cellulose acetate butyrate (CAB) as a supporting polymer was utilized for the transfer of graphene to the Si/SiO_2 substrate [11]. Post-transfer, the source and drain electrodes (10 nm Ti/ 50 nm Au) was deposited on graphene by a series of steps which include photolithography, e-beam evaporation and lift-off. E-beam evaporation was carried out using Plassys MEB 550S E-Beam evaporator. The graphene

channel was defined using photolithography and reactive ion etching (RIE) in O_2 plasma at 300 W resuting in a channel width of 50 μm. Following the channel definition, a 2 nm Al layer was deposited in O_2 ambient via e-beam evaporation. This Al layer served as the seed layer for the subsequent atomic layer deposition (ALD) of Al_2O_3. A 200°C thermal ALD process using trimethylaluminium (TMA) and H_2O as the precursors was employed for the deposition of 30 nm of Al_2O_3 which served as the top gate dielectic. Subseqently, top-gate electrode (10 nm/60 nm Ti/Au) was defined by lithography, metallisation and lift-off resulting in a top-gate channel length of 48 μm. Finally, wet etchant (HF:H_2O (1:100)) with photoresist as the etch mask was employed for selective etching of Al_2O_3 to open the vias to the source and drain electrodes.

2.3. Methodology for Pressure sensor characterisation

The presented device comprises of two components: (a) graphene field-effect transistor (GFET); (b) MIM structure with glycine/chitosan piezoelectric transducer layer. The latter is connected as extended gate to GFET (Fig. 1). The electrical response of the GFET was studied under an ambient condition using Keysight B1500A semiconductor device parameter analyser. The device response to varying pressures was studied by applying a controlled force on to β-Gly/CS piezoelectric MIM structure. The pressure was applied using an in-house setup consisting of a linear motor (VT-21 from Micronic USA) and load cell (Tedea Huntleigh Model Number 1042). The linear motor's motion was precisely controlled using the Labview program.

Results and Discussion

3.1. Glycine/Chitosan film characterisation

The crystallisation of the glycine/chitosan initiates as water begins to evaporate from the casted glycine/chitosan solution and the chitosan solution reaches the supersaturation stage. The crystallised film exhibits a spherulite morphology as depicted in the optical micrograph in Fig 3a. The spherulites contain crystal lamellae and the presence of dark amorphous regions of

chitosan between densely packed fibrils can be observed by optical microscopy (Fig. 3b). Nucleation of spherulite crystals can occur on the surface of chitosan polymer and countinued by the growth of densely branched fibrils outward from spherulite's centre to fill spherical space. Figure 3c and 3d show the SEM images of β-Gly/CS composite cross-section, revealing the oriented nanofibrils structure formed by growth of β-glycine crystals inside chitosan. The piezoelectric characteristics of the composite film are hugely influenced by the crystalline phase of the glycine crystals grown and embedded in chitosan. The XRD spectra of the synthesised glycine/chitosan film, shown in Fig. 4, depicts various planes of the β-phase glycine (JCPDS database (00-002-0171) for β-glycine). High intensity and sharp peaks indicate a perfect crystallisation of the glycine piezoelectric phase (β-phase) in synthesised composite film. The β-glycine/chitosan composite exhibited much higher stability in comparison to the standalone β-glycine crystals and no phase transformation has been observed over few months, which was confirmed by repeating the XRD measurements. The β-glycine crystals are stabilized when they are embedded in the chitosan polymer matrix and there is a possibility of intermolecular interactions between carboxyl groups of glycine molecules with amino groups of chitosan [23].

β-glycine is thermodynamically the least stable polymorph of glycine and the formation of this metastable polymorph from the liquid phase is more favourable at the higher rate of supersaturation generation and nucleation [24]. Therefore rapid crystallization should result in the formation of β-phase [25]. In glycine/chitosan solution casted on the substrate, evaporation enables the supersaturation condition and subsequently the nucleation. In the presence of the viscous solution of chitosan, the interface between primary crystal nuclei and chitosan polymer solution reduce the surface energy and affects the nucleation rate. Lower surface energy reduces the free energy barrier and induces faster nucleation [26]. Therefore, kinetic effects are dominant and controlled glycines molecular assembly in less thermodynamically stable phase

(β-form). Besides, the medium formed by chitosan polymer around initial formed crystals of β-glycine, inhibits phase transformation into the one that is more stable. These results reveal that chitosan polymer as crystallization media, plays a crutial role in controlling the polymorphism and thermodynamically stabilization of the β-phase.

3.2. Characterisation of GFET

The electrical response of GFET was studied in ambient conditions. The electrical characterisitcs of the GFET, i.e. the transfer and output characterisitics at different gate bias, are depicted in Fig 5. The transfer characterisitcs of the device show ambipolar behaviour with a Dirac voltage, which is often observed in CVD graphene channel devices. The shift in the Dirac voltage is attributed to the unintentional doping of the graphene channel, arising from the residues left during the transfer process and ambient doping [11]. The device exhibited electron and hole mobility of 467 $cm^2/V.s$ and 267 $cm^2/V.s$ respectively. The carrier mobilities of the GFET was evaluated using well estabilished diffusive transport model [27].

$$R_{total} = R_s + (L_g/We\mu\sqrt{n_0^2 + n^2}) \qquad (2)$$

where R_{total}, is the net device resistance arising due to the series resistance, R_s, and channel resistance dependent on the gate voltage. The contribution to R_s, arises from the access resistance and contact resistance. L_g and W are top-gate channel length and width of the GFET device, e is the electron charge and μ is the carrier mobility, n_0 and n are the residual carrier density and the gate bias modulated carrier density respectively given by

$$V_{TG} - V_{TG,Dirac} = \frac{ne}{C_{ox}} + \frac{\hbar v_f \pi n}{e}$$

Where v_f is the Fermi Velocity.

The sensor's dynamic response to varying pressure (5-35 kPa) was assessed using the aforementioned dynamic pressure setup. The studied pressure regime covers the pressure

experienced during daily tasks involving manipulation of objects by touching, intra-body pressure and for wearble health monitoring devices for blood pressure and pulse monitor [28].

A biasing condition of V_{ds}=50mV and V_{gs}=0V was applied to GFET during evaluation of pressure sensor. The β-glycine chitosan-based piezocapacitor was connected to the GFET, as shown in Fig. 1. The operation principle of the sensor can be described as follows: The mechanical stress due to pressure applied on the β-glycine chitosan-based piezocapacitor generates a piezopotential across the composite film, which results in the potential diference between electrodes [17]. In β-glycine crystalline structure, molecular dipole moments pointed from the NH_2-terminals to the COOH-terminals direction [29]. Applying an external pressure and deformation of the glycine/chitosan composite creates an enhanced polarization due to non-symmetrical movement of molecular dipoles in the β-glycine structure. This movement induces a potential difference between the two electrodes, which is shown as the piezoelectric output voltage. Thus, a larger deformation of the crystals due to higher pressure will lead to higher piezopotential in the β-Gly/CS film. The generated piezopotential by the external force applied on the piezocapacitor, serves as the gae bias for the GFET, where it modulates the channel carrier density resulting in observed change in channel current of the device. The application of pressure results in negative gate bias, which lead to the accumulation of holes in the graphene channel and causes an increase of the drain current. As the applied mechanical stress is removed, an opposite polarity is generated resulting in the repelling of the holes in the channel. This results in the instantaneous change in the drain current as the channel returns to its initial drain current (I_O) (Fig. 6a) The charge generated by the piezocapacitor on application of force is approximately given by:

$$Q = d_{ij}F \tag{2}$$

where d_{ij} is the piezoelectric coefficient and F is the applied force. The charge generated shows a linear relationship with the force, as per equation 2, and therefore higher magnitude of

force/pressure results in a higher of piezopotential. Consequently, higher force/pressure results in the generation of larger piezopotential and thereby the observed large change in the drain current. Fig 6a. depicts the sensor's dynamic response to a 5kPa pressure, while the response to different magnitude of pressure is shown 6b. The sensitivity of the sensor is determined by $(\Delta I/I_0)/ \Delta P$, where ΔP refers to the change in the applied pressure, ΔI is the change in the drain current for the intial value, I_0. The pressure sensor demonstrated two regime of sensitivity, at pressure range of 5kPa-20 kPa a sensitivity of $2.70 \times 10^{-4}\,kPa^{-1}$ was observed while a sensitivity of $7.56 \times 10^{-4}\,kPa^{-1}$ was observed for a pressure range between 20-35 kPa.

The improved sensitivity of the device is attributed to the improvements in the transconductance of the device as the gate voltage is increased. Therefore, the higher piezopotnetial generated at larger pressure results in a larger gate bias, eventually resulting in higher sensitivity in 20-35 kPa pressure range, as shown in Fig 6b. Table 1 provides an overview of reported sensor in comparison with various FET based sensors using an extended gate approach. Although the sensitivity of pressure sensor presented in this work is low, the higher mobility and low operation voltage are attractive features for dynamic response at higher forcing frequency where carrier mobility becomes a key factor limiting the choice of the sensors [30]. Some approaches such as Subthreshold shottky barrier thin film transistors (SB TFT) have been shown to be leading to low power (~1 nW) which is ideal for the wearbale devices [31-33]. In comparison to such approches, the reported device exhibits a higher power consumption (277 nW), however, its low operation voltage (50 mV) in comparsion to SB TFT (1 V) and higher on current are attractive features, perticularly for applications requiring higher switching speed with smaller power sources. Further, the on-current of the GFET can be modulated by channel length of the device, thereby the power consumption of the sensor can be reduced by employing larger channel length devices.

Conclusions

A low voltage GFET based dynamic pressure sensor has been presented in this paper with the biodegradable β-glycine chitosan as the transducer layer. The pressure sensor demonstrated a sensitivity of 2.70×10^{-4} kPa^{-1} for a pressure range of 5-20 kPa and 7.56×10^{-4} kPa^{-1} for a pressure range between 20-35 kPa. The low operation voltage (50 mV) and the mechanical stability of graphene could open up new avenues towards the development of low voltage flexible electronic system. Further, facile synthesis method, biocompatibility and degradability of piezoelectric layer are interesting features which could also be useful in application such as stress monitoring and wearable healthcare monitoring devices. As a way forwards, the fully degradable devices could be explored by replacing the Cu electrode in the piezoelectric transducer layer MIM with other metallic electrodes such as magnesium.

Corresponding Author

Professor Ravinder Dahiya
Tel (Off): +44 (0) 141 330 5653
*E-mail: Ravinder.Dahiya@glasgow.ac.uk

ACKNOWLEDGMENT

This work was supported in part by Engineering and Physical Sciences Research Council (EPSRC) through Engineering Fellowship for Growth - neuPRINTSKIN (EP/R029644/1), Programme Grant – Heteroprint (EP/R03480X/1) and standard grant (EP/R026173/1), and the European Commission through Marie Sklodowska-Curie Actions Fellowship - ELECTROHEAL (H2020-MSCA-IF-2016-753633)

Supporting Information: The response of piezoelectric glycine/chitosan transducer layer when pressed by touching (MP4).

REFERENCES

1. Dahiya, R.; Yogeswaran, N.; Liu, F.; Manjakkal, L.; Burdet, E.; Hayward, V.; Jörntell, H., Large-Area Soft e-Skin: The Challenges Beyond Sensor Designs. *Proceedings of the IEEE* **2019,** *107* (10), 2016-2033.

2. Dahiya, R. S.; Valle, M., *Robotic tactile sensing: technologies and system*. Springer Science & Business Media: Dordrecht,, 2013.
3. Adami, A.; Dahiya, R. S.; Collini, C.; Cattin, D.; Lorenzelli, L., POSFET touch sensor with CMOS integrated signal conditioning electronics. *Sensors and Actuators A: Physical* **2012,** *188*, 75-81.
4. Sun, Q.; Kim, D. H.; Park, S. S.; Lee, N. Y.; Zhang, Y.; Lee, J. H.; Cho, K.; Cho, J. H., Transparent, Low-Power Pressure Sensor Matrix Based on Coplanar-Gate Graphene Transistors. *Advanced Materials* **2014,** *26* (27), 4735-4740.
5. Nela, L.; Tang, J.; Cao, Q.; Tulevski, G.; Han, S.-J., Large-Area High-Performance Flexible Pressure Sensor with Carbon Nanotube Active Matrix for Electronic Skin. *Nano Letters* **2018,** *18* (3), 2054-2059.
6. Gupta, S.; Shakthivel, D.; Lorenzelli, L.; Dahiya, R., Temperature Compensated Tactile Sensing Using MOSFET With P(VDF-TrFE)/BaTiO3 Capacitor as Extended Gate. *IEEE Sensors Journal* **2019,** *19* (2), 435-442.
7. Someya, T.; Sekitani, T.; Iba, S.; Kato, Y.; Kawaguchi, H.; Sakurai, T., A large-area, flexible pressure sensor matrix with organic field-effect transistors for artificial skin applications. *Proceedings of the National Academy of Sciences of the United States of America* **2004,** *101* (27), 9966-9970.
8. Yeo, S. Y.; Park, S.; Yi, Y. J.; Kim, D. H.; Lim, J. A., Highly Sensitive Flexible Pressure Sensors Based on Printed Organic Transistors with Centro-Apically Self-Organized Organic Semiconductor Microstructures. *ACS Applied Materials & Interfaces* **2017,** *9* (49), 42996-43003.
9. Zang, Y.; Zhang, F.; Huang, D.; Gao, X.; Di, C.-a.; Zhu, D., Flexible suspended gate organic thin-film transistors for ultra-sensitive pressure detection. *Nature Communications* **2015,** *6* (1), 6269.
10. Kim, D.-I.; Quang Trung, T.; Hwang, B.-U.; Kim, J.-S.; Jeon, S.; Bae, J.; Park, J.-J.; Lee, N.-E., A Sensor Array Using Multi-functional Field-effect Transistors with Ultrahigh Sensitivity and Precision for Bio-monitoring. *Scientific Reports* **2015,** *5* (1), 12705.
11. Yogeswaran, N.; Navaraj, W. T.; Gupta, S.; Liu, F.; Vinciguerra, V.; Lorenzelli, L.; Dahiya, R., Piezoelectric graphene field effect transistor pressure sensors for tactile sensing. *Applied Physics Letters* **2018,** *113* (1), 014102.
12. Dahiya, R. S.; Adami, A.; Collini, C.; Lorenzelli, L., POSFET tactile sensing arrays using CMOS technology. *Sensors and Actuators A: Physical* **2013,** *202*, 226-232.
13. Dagdeviren, C.; Su, Y.; Joe, P.; Yona, R.; Liu, Y.; Kim, Y.-S.; Huang, Y.; Damadoran, A. R.; Xia, J.; Martin, L. W.; Huang, Y.; Rogers, J. A., Conformable amplified lead zirconate titanate sensors with enhanced piezoelectric response for cutaneous pressure monitoring. *Nature Communications* **2014,** *5* (1), 4496.
14. Vishniakou, S.; Chen, R.; Ro, Y. G.; Brennan, C. J.; Levy, C.; Yu, E. T.; Dayeh, S. A., Improved Performance of Zinc Oxide Thin Film Transistor Pressure Sensors and a Demonstration of a Commercial Chip Compatibility with the New Force Sensing Technology. *Advanced Materials Technologies* **2018,** *3* (3), 1700279.
15. Wu, W.; Wen, X.; Wang, Z. L., Taxel-Addressable Matrix of Vertical-Nanowire Piezotronic Transistors for Active and Adaptive Tactile Imaging. *Science* **2013,** *340* (6135), 952-957.
16. Chen, Z.; Wang, Z.; Li, X.; Lin, Y.; Luo, N.; Long, M.; Zhao, N.; Xu, J.-B., Flexible Piezoelectric-Induced Pressure Sensors for Static Measurements Based on Nanowires/Graphene Heterostructures. *ACS Nano* **2017,** *11* (5), 4507-4513.
17. Gupta, S.; Yogeswaran, N.; Giacomozzi, F.; Lorenzelli, L.; Dahiya, R., Touch Sensor based on Flexible AlN Piezocapacitor Coupled with MOSFET. *IEEE Sensors Journal* **2019**, 1-1.
18. Jackson, N.; Keeney, L.; Mathewson, A., Flexible-CMOS and biocompatible piezoelectric AlN material for MEMS applications. *Smart Materials and Structures* **2013,** *22* (11), 115033.
19. Curry, E. J.; Ke, K.; Chorsi, M. T.; Wrobel, K. S.; Miller, A. N.; Patel, A.; Kim, I.; Feng, J.; Yue, L.; Wu, Q.; Kuo, C.-L.; Lo, K. W.-H.; Laurencin, C. T.; Ilies, H.; Purohit, P. K.; Nguyen, T. D., Biodegradable Piezoelectric Force Sensor. *Proceedings of the National Academy of Sciences* **2018,** *115* (5), 909-914.
20. Rajala, S.; Siponkoski, T.; Sarlin, E.; Mettänen, M.; Vuoriluoto, M.; Pammo, A.; Juuti, J.; Rojas, O. J.; Franssila, S.; Tuukkanen, S., Cellulose Nanofibril Film as a Piezoelectric Sensor Material. *ACS Applied Materials & Interfaces* **2016,** *8* (24), 15607-15614.
21. Hosseini, E. S.; Manjakkal, L.; Shakthivel, D.; Dahiya, R., Glycine–Chitosan-Based Flexible Biodegradable Piezoelectric Pressure Sensor. *ACS applied materials & interfaces* **2020,** *12* (8), 9008-9016.
22. Guerin, S.; Stapleton, A.; Chovan, D.; Mouras, R.; Gleeson, M.; McKeown, C.; Noor, M. R.; Silien, C.; Rhen, F. M. F.; Kholkin, Andrei L.; Liu, N.; Soulimane, T.; Tofail, S. A. M.; Thompson, D., Control of piezoelectricity in amino acids by supramolecular packing. *Nature Materials* **2018,** *17* (2), 180-186.
23. Ibrahim, M. A.; Gawad, A. E.-D. A., Spectroscopic Analyses of Chitosan Interactions with Amino Acids. *Journal of Computational and Theoretical Nanoscience* **2012,** *9* (8), 1120-1124.
24. He, G.; Wong, A. B. H.; Chow, P. S.; Tan, R. B. H., Effects of the rate of supersaturation generation on polymorphic crystallization of m-hydroxybenzoic acid and o-aminobenzoic acid. *Journal of Crystal Growth* **2011,** *314* (1), 220-226.
25. Jiang, Q.; Ward, M. D., Crystallization under nanoscale confinement. *Chemical Society Reviews* **2014,** *43* (7), 2066-2079.

26. Sosso, G. C.; Chen, J.; Cox, S. J.; Fitzner, M.; Pedevilla, P.; Zen, A.; Michaelides, A., Crystal Nucleation in Liquids: Open Questions and Future Challenges in Molecular Dynamics Simulations. *Chemical Reviews* **2016,** *116* (12), 7078-7116.
27. Kim, S.; Nah, J.; Jo, I.; Shahrjerdi, D.; Colombo, L.; Yao, Z.; Tutuc, E.; Banerjee, S. K., Realization of a high mobility dual-gated graphene field-effect transistor with Al2O3 dielectric. *Applied Physics Letters* **2009,** *94* (6), 062107.
28. Zang, Y.; Zhang, F.; Di, C.-a.; Zhu, D., Advances of flexible pressure sensors toward artificial intelligence and health care applications. *Materials Horizons* **2015,** *2* (2), 140-156.
29. Bystrov, V. S.; Seyedhosseini, E.; Bdikin, I.; Kopyl, S.; Neumayer, S. M.; Coutinho, J.; Kholkin, A. L., Bioferroelectricity in Nanostructured Glycine and Thymine: Molecular Modeling and Ferroelectric Properties at the Nanoscale. *Ferroelectrics* **2015,** *475* (1), 107-126.
30. Hannah, S.; Davidson, A.; Glesk, I.; Uttamchandani, D.; Dahiya, R.; Gleskova, H., Multifunctional sensor based on organic field-effect transistor and ferroelectric poly (vinylidene fluoride trifluoroethylene). *Organic Electronics* **2018,** *56*, 170-177.
31. Taalla, R. V.; Arefin, M. S.; Kaynak, A.; Kouzani, A. Z., A review on miniaturized ultrasonic wireless power transfer to implantable medical devices. *IEEE access* **2018,** *7*, 2092-2106.
32. Jiang, C.; Choi, H. W.; Cheng, X.; Ma, H.; Hasko, D.; Nathan, A., Printed subthreshold organic transistors operating at high gain and ultralow power. *Science* **2019,** *363* (6428), 719-723.
33. Lee, S.; Nathan, A., Subthreshold Schottky-barrier thin-film transistors with ultralow power and high intrinsic gain. *Science* **2016,** *354* (6310), 302-304.

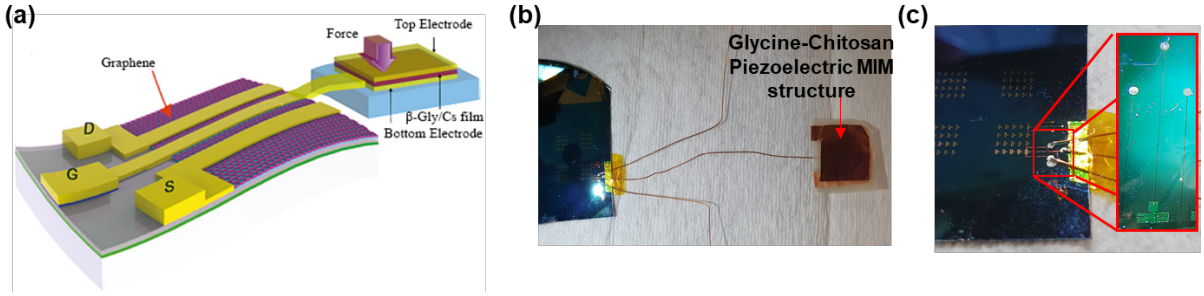

Figure 1. Pressure sensor comprising a GFET with a glycine-chitosan piezoelectric transducer layer (a)The scheme of GFET coupled with glycine/chitosan in an extended gate configuration. (b-c) Glycine-Chitosan MIM structure connected in an extended gate configuration to the GFET. The inset in (c) shows the contact pads to the GFET.

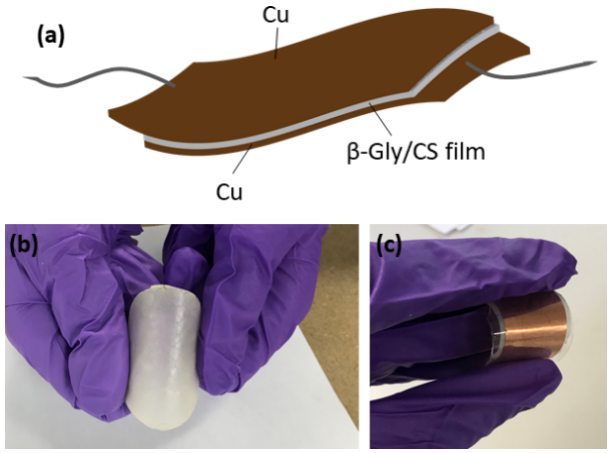

Figure 2. (a) Schematic illustration of β-glycine/chitosan MIM structure. (b, c) Optical image of fabricated flexible β-glycine/chitosan film and β-glycine/chitosan MIM structure encapsulated by Cu electrodes and PDMS.

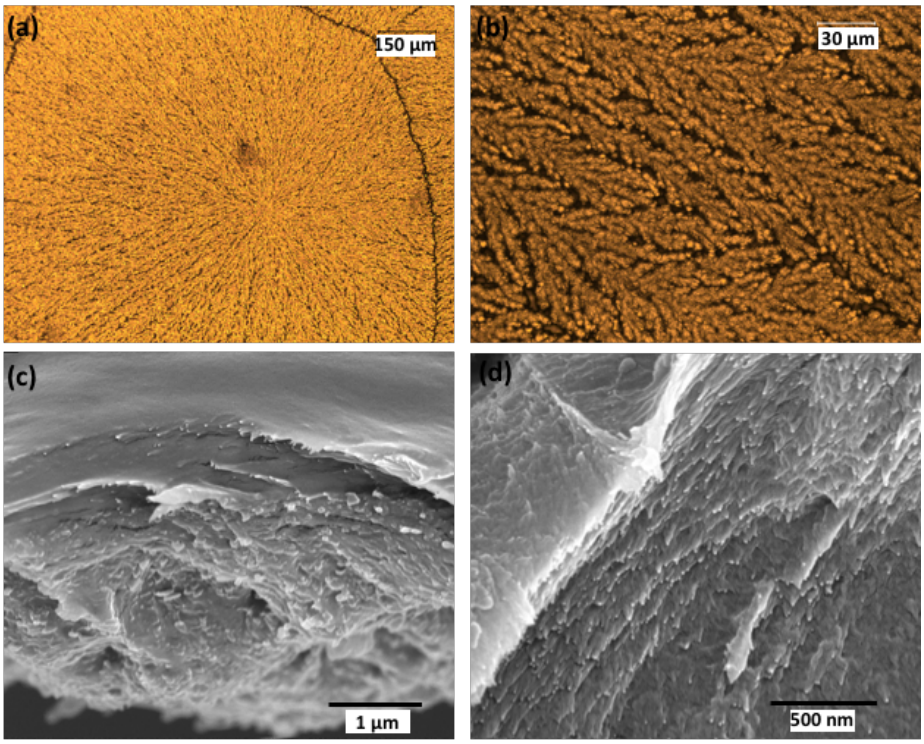

Figure 3. (a) and (b) Optical micrograph of showing the morphology of β-glycine/chitosan film, (c) and (d) SEM images over the cross section of the film showing nanofibrils structure of β-glycine/chitosan composite.

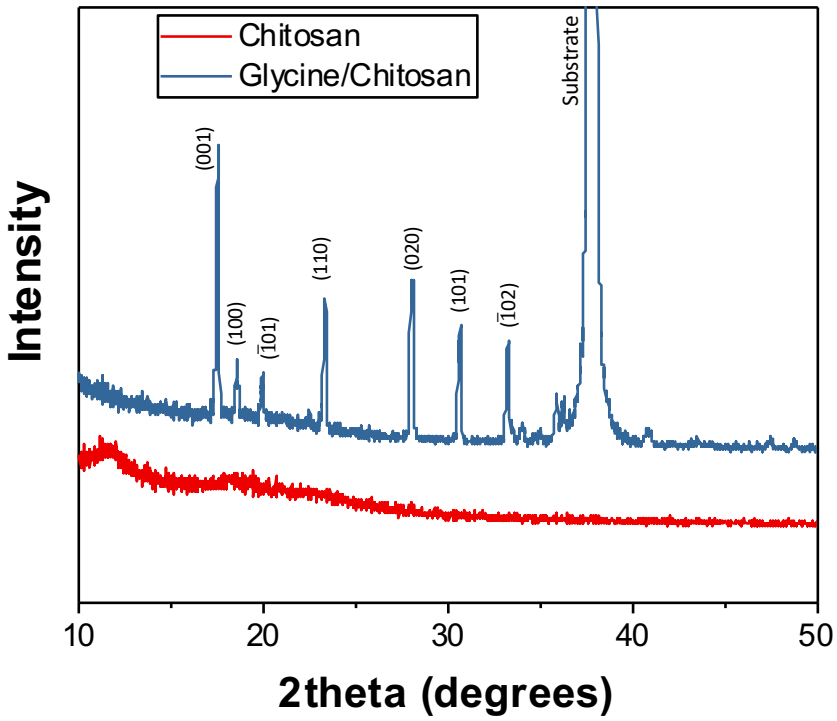

Figure 4. XRD pattern of pure chitosan (red) and glycine/chitosan (blue) composite with 0.8:1 glycine to chitosan ratio.

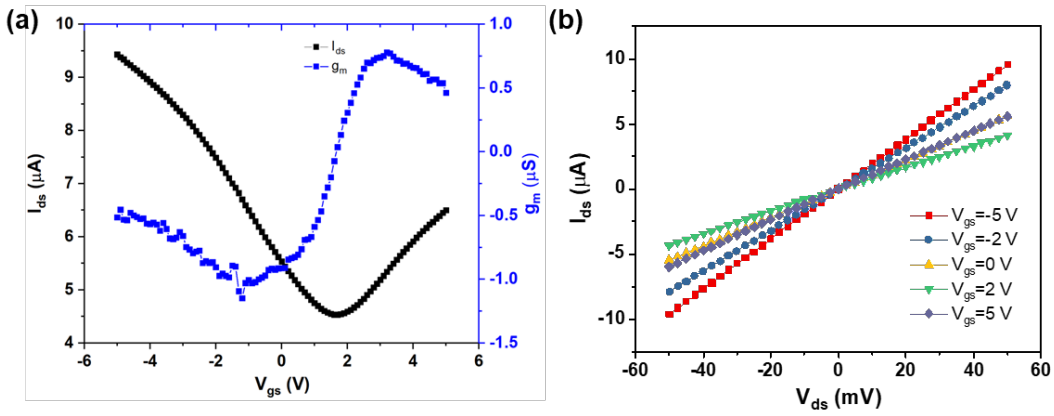

Figure 5. Electrical response of GFET. (a) Transfer characteristics of GFET at V_{ds}=50 mV and (b) Output characteristics of GFET for different top-gate bias.

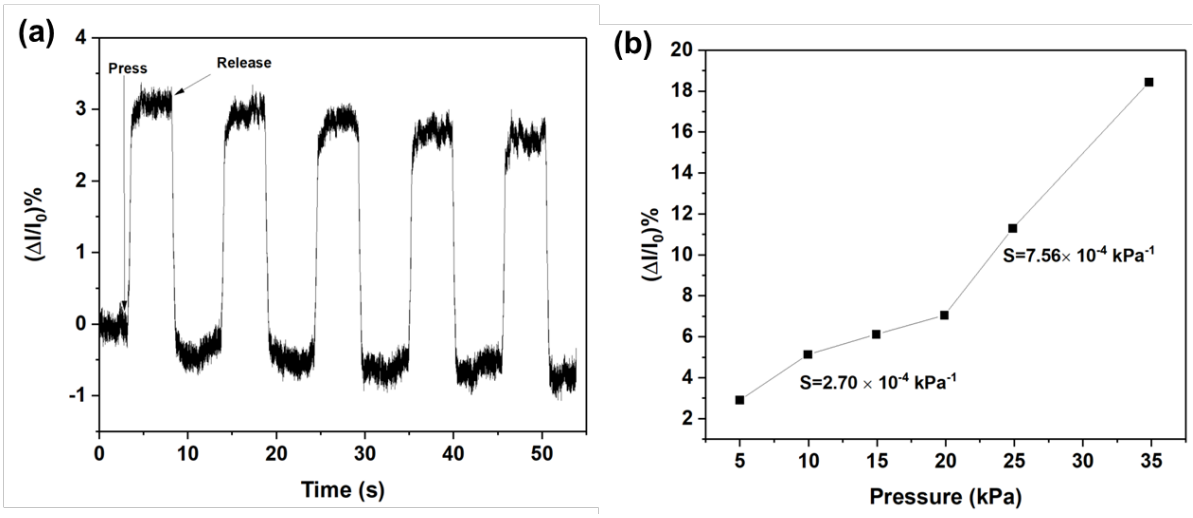

Figure 6. (a) The dynamic response of the sensor for a pressure of 5 kPa. The press event indicates the application of pressure to the β-Gly/CS MIM structure and release event indicates the release of force from the β-Gly/CS MIM structure. (b) Normalised change in current vs pressure, the device exhbit an improved sensitivity at higher pressure (<20 kPa).

Table 1. Comparison of FET based sensors with different piezoelectric transducer layer in extended gate configuration.

FETs structure	Extended gate structure	Operating Voltage (V)	Carrier Mobility ($cm^2/V.s$)	Pressure range (kPa)	Sensitivity (GPa^{-1})
OFET (DNTT) [30]	Non biodegradable P(VDF-TrFE)	$V_{ds} = V_{gs} = -2$	0.56	0–320	1.96
MOSFET [17]	Non-biodegradable AlN	$V_{ds} = V_{gs} = 1$	695	5-35	264000
GFET [11]	Non-biodegradable PZT	$V_{ds} = 0.1$; $V_{gs} = 0$	$\mu_h = 879$ $\mu e = 828$	0–94.18	4550
GFET (this work)	Biodegradable Glycine/ Chitosan	$V_{ds} = 0.05$; $V_{gs} = 0$	$\mu_h = 467$ $\mu_e = 267$	5–20 20–35	270 756

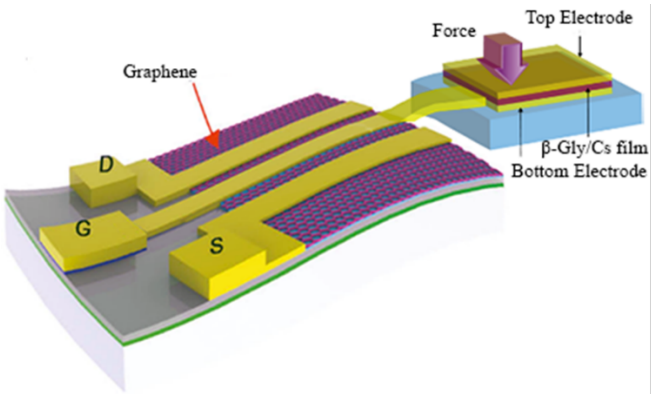
Force
Top Electrode
Graphene
β-Gly/Cs film
Bottom Electrode
D
G
S

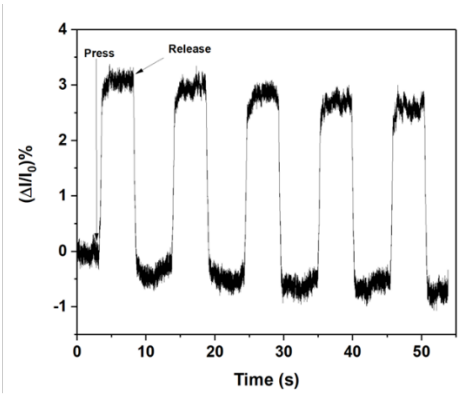
Press
Release
(ΔI/I0)%
Time (s)
4
3
2
1
0
-1
0
10
20
30
40
50

TOC Figure